JOURNAL OF COMPUTATIONAL PHYSICS 61, 321–344 (1985)

Numerical Methods for the Transition to Wavy Taylor Vortices

C. A. JONES

School of Mathematics, University of Newcastle upon Tyne NE1 7RU, England

Received May 23, 1984; revised January 22, 1985

Numerical methods for the analysis of the nonaxisymmetric stability of two-dimensional axisymmetric flows are discussed. The relative merits of a fully spectral approach are compared with methods which are spectral in one direction and finite difference in the other. The results are applied to the onset of waviness in Taylor vortices; it is shown that the methods described are capable of finding accurate eigenvalues for Taylor numbers up to fifty times critical.

1. INTRODUCTION

The physical problem which gives rise to the calculations described in this paper is the flow of incompressible fluid between concentric rotating cylinders. Taylor–Couette flow undergoes a series of transitions as the rotation rate, as measured by the dimensionless Taylor number, is increased.

The first transition, at $Ta = Ta_c$, is generally from purely azimuthal flow to axisymmetric toroidal vortices; this is the transition first studied by Taylor [32]. These toroidal vortices have been studied by many workers using different means: weakly nonlinear expansions have been developed by Davey [5], Eagles [10], and others; many numerical calculations have been performed, among them those of Meyer [22], Rogers and Beard [31], Meyer-Spasche and Keller [23], Jones [17, 18], and Booz [2]; there is also a large literature, which has recently been reviewed by DiPrima and Swinney [7]. Most, but not all, of the theoretical work has used the infinite cylinder approximation.

As the rotation rate is further increased, the toroidal vortices generally lose their axial symmetry, and become wavy at some critical Taylor number, Ta_w. This transition was first analysed theoretically using weakly nonlinear expansions by Davey, DiPrima, and Stuart [6], and was subsequently investigated by Nakaya [26] and Jones [17, 18].

In a previous paper [17] the author predicted a rapid rise in the critical Taylor number, Ta_w, for the onset of waves as the radius ratio η is reduced below $\eta = 0.78$. This prediction has been confirmed by laboratory experiments, such as those of Cole [4] and Park [28]. Also calculations of the wave speeds near Ta_w were in reasonable agreement with observations; see also King *et al.* [19]. However, the

0021-9991/85 $3.00

581/61/2-9

work in [17] was limited by the fact that the numerical methods used only gave really reliable results for Taylor numbers $\leqslant 10Ta_c$. Since many interesting experiments on the wavy vortex transition have been done at higher Taylor numbers than this, e.g., Lorenzen, Pfister, and Mullin [20] and Cole [4], new numerical techniques are needed to explore these regimes.

This paper contains a description of the numerical methods used in Jones [17], and compares them with a new method which can reach Taylor numbers substantially in excess of $10Ta_c$. Since the agreement between theory and observation is generally rather good in Taylor–Couette flow, there is a need for a higher level of precision in the numerical calculations than is generally required for numerical fluid dynamics. Also, accurate calculations of the transition points serve as useful "benchmark" checks for time-dependent calculations such as those of Moser, Moin, and Leonard [24] and Marcus [21].

The numerical problem involved in finding Ta_w and the corresponding wave speed, c, consists of two parts. First we must calculate the nonlinear axisymmetric Taylor vortices. The method used here was a spectral method, together with Newton–Raphson iterations to solve the resulting nonlinear algebraic equations. Details are given in Section 3. The second part of the problem is then to perform a linear stability analysis about the nonlinear states. This involves solving a two-dimensional eigenvalue problem, in the axial and radial directions, with prescribed boundary conditions. Since the ϕ-dependence for the eigenvalue problem is $\propto e^{im\phi}$, the coefficients are complex, and there are really two eigenvalues, Ta_w and c, the wave speed. It is, however, generally more convenient (and in this problem more instructive) to let Ta be a parameter and solve for the complex growth rate, $\sigma + i\omega$, and then adjust Ta until $\sigma = 0$. This system is of sixth order in space, with three boundary conditions applied at each boundary.

There are, of course, a great many different techniques for solving 2-D eigenvalue problems of this type. The particular features of this Taylor–Couette problem (and also of similar problems in fluid dynamics, such as the convection problem) are the high differential order and the non-Hermitian character of the problem; eigenvalues do not occur in complex conjugate pairs. We first consider how we are going to represent the scalar fields occurring in the problem. Three possibilities have been considered: spectral representations in the radial and axial directions, which we call an SS method, spectral representation in one direction and finite difference representation in the other, which we call an SF method, and finite difference representation in both directions, which we call an FF method. Finite element methods were not considered, although they may well prove to be competitive in these types of problems. For studying bifurcations in fluid dynamics SS methods have been used extensively (e.g., Clever and Busse [3], Nagata and Busse [25]), but FF methods have also been used (e.g., Fearn and Proctor [12]). The most successful method at the higher Taylor numbers found here was of mixed SF type.

Having decided on the method of representation, we have to select the most appropriate formulation of the sixth-order system. The equations can be formulated in terms of two dependent variables, one equation of fourth order and the other of

second order. This can, in fact, be done in several different ways. This would appear to be the optimum formulation when using fully spectral methods (SS), where the fourth-order derivatives do not create too great a problem, and the need to minimise the order of the matrices is at a premium. With finite difference representations, it was felt to be better to use three dependent variables involving only second-order derivatives. Details of how the equations are formulated are given in Section 2.

We must next decide on how we are going to find the eigenvalues from the resulting matrices. An SS method leads to dense matrices; but if the expansion functions are well chosen, the order of the matrices will be much smaller than that for finite difference methods of equivalent accuracy. At low Taylor number, the eigenfunctions are extremely smooth, so that SS methods can give good results even when the truncation is very severe; we can then use the LR algorithm to find all the eigenvalues (and eigenvectors if required) of our comparatively small dense matrices. We can then select the most unstable (or least stable) eigenvalues and follow these up to higher values of the Taylor number.

SF and FF methods lead to matrices of varying degrees of sparseness; inverse iteration (e.g., Wilkinson [33]) was the basis of the most successful method tried here. The numerical evidence suggests that the eigenvalues for this problem are always well separated in the complex plane: as we proceed by slowly varying the parameters, good estimates are usually available for the trial eigenvalue.

When sparse matrices are involved, the choice of sparse matrix solver for performing the LU decomposition is important. In the SF method, the sparsity pattern consists of dense rectangular blocks down the leading diagonal. The so-called "frontal" methods (e.g., Duff [9]) were found to be very effective. The FF methods lead to a more complicated sparsity pattern, which is not so easy to take full advantage of; this is particularly significant if we wish to vectorize the inner loops of LU decomposition (Duff and Reid, [8]). This is the main reason why we were unable to make FF methods competitive with SF methods for this problem.

The decision between SS methods and SF methods is more complicated. Although the flows are extremely smooth at low Taylor number, at higher Ta boundary layer structures begin to develop (Batchelor [1]). A similar situation occurs in Rayleigh–Benard convection (Roberts [29, 30]). For the Taylor case, Batchelor's argument gives the boundary layer thickness, δ, $\sim Ta^{-1/4}$ at large Ta. This scaling applies both to the boundary layers near the cylindrical sidewalls and also to the internal boundary layers which develop between each toroidal cell (e.g., Fasel and Booz [11]). In consequence, as Ta increases, more spectral functions are required to maintain the resolution. Naturally, the number of finite difference mesh points has to be increased too; indeed, if we denote the number of spectral functions required in each direction by N_S and the number of finite difference mesh points by N_F, then N_S/N_F shows no tendency to increase. Indeed, in the radial direction the zeros of suitable spectral functions are concentrated in the boundary layers, so that N_S/N_F is likely to decrease as Ta is increased. We might therefore suppose that the fully spectral methods would be much preferred at higher Ta. However, for the SS

method, the time taken for inverting the full matrix grows very rapidly with N_S ($\sim N_S^6$), whereas for the SF method, the time taken for inversion grows at the less rapid rate of $N_S^3 N_F$. In consequence, although SS methods involve considerably smaller matrices at higher Ta than SF methods, SF methods were found to consume less CPU time than SS methods to achieve the desired accuracy. At low Ta, the N_S required to give accurate solutions may be quite small, so the penalty for inverting full matrices is correspondingly less. We find that SS is then preferred to SF at low Ta. The crossover point, at which both methods are comparable, will depend on the computer used and the budget available (see Section 5).

When spectral representation is used, we must decide on the set of functions to be employed. In this work, Chebyshev polynomials are used for the nonperiodic r-direction, and trigonometric functions are used in the periodic z-direction. Choices other than Chebyshev polynomials have been used by other authors, e.g., Clever and Busse [3] used the Chandrasekhar–Reid functions, but the uniform spacing of the zeros of these functions near the boundaries makes their convergence properties less effective; see Orszag [27]. Another possibility is expansion in Legendre polynomials (Hussaini, Salas, and Zang [14] and Zang, Wong, and Hussaini [34]) which are as convenient to use as Chebyshev polynomials, and also have a high density of zeros near the boundaries.

The detailed comparison of the results of the computations with the laboratory experiments is given in Jones [16].

2. Formulation of the Equations

In vector form the incompressible Navier–Stokes equations are

$$\frac{\partial \mathbf{u}}{\partial t} + (\mathbf{u} \cdot \nabla)\,\mathbf{u} = -\frac{1}{\rho}\nabla p + \nu \nabla^2 \mathbf{u} \tag{2.1}$$

$$\nabla \cdot \mathbf{u} = 0. \tag{2.2}$$

In cylindrical polar coordinates (r, ϕ, z) a natural formulation of the nonlinear axisymmetric Navier–Stokes equations is in terms of the stream-function ψ, defined so that

$$(u_r, u_\phi, u_z) = \left(-\frac{1}{r}\frac{\partial \psi}{\partial z}, u_\phi, \frac{1}{r}\frac{\partial \psi}{\partial r} \right). \tag{2.3}$$

Then the potential vorticity, Z, is defined by

$$Z = -\frac{1}{r}\frac{\partial}{\partial r}\frac{1}{r}\frac{\partial \psi}{\partial r} - \frac{1}{r^2}\frac{\partial^2 \psi}{\partial z^2}. \tag{2.4}$$

Before the onset of Taylor vortices the Couette velocity field is azimuthal,

$$u_\phi = \frac{\Omega_1 R_2^2}{d(R_1 + R_2)} \left[\frac{(1-\mu) R_1^2}{r} - (\eta^2 - \mu)\, r \right] = u_\phi^0(r) \tag{2.5}$$

where R_1 and R_2 are the radii of the inner and outer cylinders, $\eta = R_1/R_2$, Ω_1 and Ω_2 are the angular velocities of the inner and outer cylinders, $d = R_2 - R_1$, and $\mu = \Omega_2/\Omega_1$. In the case of counter-rotating cylinders, μ is $-ve$. The results reported here concern only the case $\mu = 0$, i.e., the outer cylinder is at rest.

We define v, the departure of the azimuthal flow field from the basic Couette flow field, by

$$v = u_\phi - u_\phi^0(r). \tag{2.6}$$

The equations are then nondimensionalized by using these transformations for the dependent variables

$$\psi \to \psi \nu R_2; \qquad Z \to \frac{\nu Z}{d^2 R_2}; \qquad v \to \Omega_1 R_1 v,$$

where ν is the kinematic viscosity.

For the independent variables we define x, ζ such that $z = \zeta d$ and $r = R_1 + xd$, so the cylinders are at $x = 0$ and $x = 1$. We introduce $\hat{r}$ such that $\hat{r} = \eta + x(1-\eta) = (1-\eta)\, r/d$.

The axisymmetric Navier–Stokes equations then become

$$-\frac{1}{\hat{r}}\frac{\partial}{\partial x}\frac{1}{\hat{r}}\frac{\partial \psi}{\partial x} - \frac{1}{\hat{r}^2}\frac{\partial^2 \psi}{\partial \zeta^2} = Z \tag{2.7}$$

$$\frac{\partial \psi}{\partial x}\frac{\partial Z}{\partial \zeta} - \frac{\partial \psi}{\partial \zeta}\frac{\partial Z}{\partial x} + \frac{\eta Ta}{1-\eta}\frac{\partial v}{\partial \zeta}\left\{1 - \frac{(1-\mu)\,\eta^2}{(\eta^2-\mu)\,\hat{r}^2} - \frac{\eta(1-\eta^2)\,v}{\hat{r}(\eta^2-\mu)}\right\}$$
$$= \frac{\partial}{\partial x}\frac{1}{\hat{r}}\frac{\partial}{\partial x}(\hat{r}^2 Z) + \hat{r}\frac{\partial^2 Z}{\partial \zeta^2} \tag{2.8}$$

$$\frac{\partial \psi}{\partial x}\frac{\partial v}{\partial \zeta} - \frac{\partial \psi}{\partial \zeta}\frac{\partial v}{\partial x} + \frac{\partial \psi}{\partial \zeta}\left\{\frac{2(\eta^2-\mu)}{\eta(1+\eta)} - \frac{(1-\eta)\,v}{\hat{r}}\right\}$$
$$= \hat{r}\left[\frac{\partial^2 v}{\partial \zeta^2} + \frac{\partial}{\partial x}\frac{1}{\hat{r}}\frac{\partial}{\partial x}(v\hat{r})\right] \tag{2.9}$$

where

$$Ta = \frac{2\Omega_1^2 d^4(\eta^2-\mu)}{(1-\eta^2)\,\nu^2} = \frac{2\Omega_1 d^3(\Omega_1 R_1^2 - \Omega_2 R_2^2)}{\nu^2(R_1+R_2)}.$$

Another commonly used set of dimensionless parameters are the inner and outer Reynolds numbers, defined by $R_i = \Omega_1 R_1 (d/\nu)$ and $R_o = \Omega_2 R_2 (d/\nu)$. These are simply related to Ta and μ, since

$$R_i = \left\{\frac{\eta^2(1+\eta)\,Ta}{2(1-\eta)(\eta^2-\mu)}\right\}^{1/2}; \qquad R_o = \left\{\frac{\mu^2(1+\eta)\,Ta}{2(1-\eta)(\eta^2-\mu)}\right\}^{1/2}.$$

In the case where the outer cylinder is at rest, it is common to define $R_i = \mathrm{Re}$ as the Reynolds number. The boundary conditions to be applied are

$$\psi = \frac{\partial \psi}{\partial x} = v = 0 \qquad \text{on } x = 0, 1 \tag{2.10}$$

and ψ, v are periodic in ζ, with period $2\pi/\alpha$. The system is of sixth order.

Once the steady-state axisymmetric equations (2.7) to (2.9) have been solved, we can examine the stability of the solution by solving the small disturbance equations

$$\frac{\partial \mathbf{u}'}{\partial t} + (\mathbf{u}^\circ \cdot \nabla)\,\mathbf{u}' + (\mathbf{u}' \cdot \nabla)\,\mathbf{u}^\circ = -\frac{1}{\rho}\nabla p' + \nu \nabla^2 \mathbf{u}' \tag{2.11}$$

$$\nabla \cdot \mathbf{u}' = 0. \tag{2.12}$$

There are various ways of reducing these vector equations to a form suitable for numerical solution, depending on the numerical method to be employed. For axisymmetric disturbances, it is convenient to formulate the equation in stream-function and vorticity form, i.e., to follow the same procedure as led to Eqs. (2.7) to (2.9). However, for nonaxisymmetric disturbances we have no stream-function and a different procedure must be adopted. If the numerical method is of SS type, it is important to reduce the number of dependent variables to a minimum in order to minimise the order of the resulting matrices. Since differentiation is then a comparatively simple and accurate procedure, the high-order derivatives resulting from eliminating dependent variables cause no problems.

The nondimensionalization of the asymmetric perturbation equations follows that of the axisymmetric equations;

$$u_r' \to \frac{\nu u_r'}{d}; \qquad u_z' \to \frac{\nu u_z'}{d}; \qquad u_\phi' \to \Omega_1 R_1 u_\phi'; \qquad p' \to \frac{p' \nu^2}{d^2}\rho$$

are the scalings for the dependent variables: we also use $t \to (d^2/\nu)\,t$ for the time scale, and $\phi \to \{2(\eta^2 - \mu)/(1-\eta^2)\,Ta\}^{1/2}\,\hat{\phi}$ for the azimuthal angle. If disturbances are $\propto e^{im\phi}$, m an integer, then in the stretched coordinate $\hat{\phi}$, disturbances are $\propto e^{ik\hat{\phi}}$, where $k = m\{Ta(1-\eta^2)/2(\eta^2 - \mu)\}^{1/2}$. k then has discrete values, but not necessarily integer values. The introduction of k rather than m may seem to be perverse, but in the narrow-gap limit $\eta \to 1$ it is k, and not m, which remains finite: so introducing k permits us to solve the equations for $\eta = 1$. We also note that $\mathbf{u}'$ and p' are complex quantities.

When SS methods were used, the two dependent variables θ and χ were defined by

$$\mathbf{u} = \nabla \times \theta \hat{\mathbf{r}} + \nabla \times \nabla \times \chi \hat{\mathbf{r}}, \qquad \hat{\mathbf{r}} \text{ being the unit vector in the } r\text{-direction,} \tag{2.13}$$

an expansion related to separation into toroidal and poloidal fields. An advantage of this procedure is that the equations derived are nonsingular in the axisymmetric limit $k \to 0$. The pressure is eliminated by taking the curl of the momentum equations. The two equations are derived by taking the r-component of the curl of Eq. (2.13) and the r-component of curl^2 of Eq. (2.13). The boundary conditions are

$$\chi = \frac{\partial \chi}{\partial x} = \theta = 0 \qquad \text{on } x = 0, 1 \tag{2.14}$$

together with periodic conditions on χ and θ in the ζ-direction.

When SF methods are used, we want to avoid fourth derivatives if possible. We therefore formulated the equations in terms of u'_r, u'_z, and p', the pressure perturbation. We then split the sixth-order system into three second-order systems. The divergence of the momentum equation (2.11) gives

$$\nabla^2 p' = -2 \operatorname{div}[(\mathbf{u}' \cdot \nabla)\, \mathbf{u}^\circ] \tag{2.15}$$

using the identity $\operatorname{div}[(\mathbf{u}^0 \cdot \nabla)\, \mathbf{u}'] = \operatorname{div}[(\mathbf{u}' \cdot \nabla)\, \mathbf{u}^\circ]$. We eliminate u'_ϕ using the continuity equation, and take the radial and vertical momentum components as the other two equations. We obtain

$$\frac{\partial u'_r}{\partial t} + (\mathbf{u}^\circ \cdot \nabla_\perp)\, u'_r + (\mathbf{u}' \cdot \nabla_\perp)\, u^\circ_r + \frac{imu^\circ_\phi u'_r}{r} - \frac{2i}{m} u^\circ_\phi \nabla_\perp \cdot \mathbf{u}'$$

$$= -\frac{1}{\rho}\frac{\partial p'}{\partial r} + \nu\left[\nabla^2 u'_r - \frac{u'_r}{r^2} + 2\nabla_\perp \cdot \mathbf{u}'\right] \tag{2.16}$$

$$\frac{\partial u'_z}{\partial t} + (\mathbf{u}^\circ \cdot \nabla_\perp)\, u'_z + (\mathbf{u}' \cdot \nabla_\perp)\, u^\circ_z + \frac{imu^\circ_\phi u'_z}{r} = -\frac{1}{\rho}\frac{\partial p'}{\partial z} + \nu \nabla^2 u'_z. \tag{2.17}$$

Here $\nabla_\perp$ denotes the operator $(\partial/\partial r,\ \partial/\partial z)$ and $\nabla_\perp \cdot \mathbf{u}'$ denotes $(1/r)(\partial/\partial r)(ru'_r) + \partial u'_z/\partial z$. We note that as (2.16) contains terms in $1/m$, only non-axisymmetric modes can be treated by this formulation. We cast (2.15), (2.16), and (2.17) into dimensionless form using the same scalings as before. The boundary conditions are

$$u'_r = \frac{\partial u'_r}{\partial x} = u'_z = 0 \tag{2.18}$$

on both the inner and outer boundaries, together with periodic conditions in the ζ-direction.

3. Method Used for Axisymmetric Equations

We now briefly describe the technique used to solve Eqs. (2.7) to (2.9) (see also [17]). The method adopted was fully spectral, that is, of SS type. We write

$$\psi = \sum_{n=1}^{N} \sum_{m=0}^{M} \psi_{mn} T_m^*(x) \sin n\alpha\zeta$$
$$v = \sum_{n=0}^{N} \sum_{m=0}^{M} v_{mn} T_m^*(z) \cos n\alpha\zeta \tag{3.1}$$

where $T_m^*(x)$ is the mth Chebyshev polynomial defined on $0 \leqslant x \leqslant 1$. We eliminate Z from Eq. (2.8), using (2.7), so no expansion is required for Z. N and M are the truncation parameters in the ζ and x directions, respectively. We now must find the $(M+1)(2N+1)$ coefficients ψ_{mn} and v_{mn}. Substituting (3.1) into the boundary conditions (2.10) gives $6N+2$ equations. The remaining $(M-3)N+(M-1)(N+1)$ equations can be found by collocation. This method is simple to program and is particularly suitable when the coefficients are complicated.

For the ψ equation (2.8), we set up an $(M-3)\times N$ mesh, with mesh points at x-values given by the zeros of $T_{M-3}^*(x)$ and ζ-values given by the zeros of $\cos(N+1)\alpha\zeta$. (Note that some authors use the zeros of $U_n^*(x)$, the Chebyshev polynomials of the second kind, in preference to those of $T_n^*(x)$.) We then require that Eq. (2.8) be satisfied exactly at each of these $(M-3)$ mesh points, thus obtaining $(M-3)N$ equations.

In the program, the equations are solved by Newton–Raphson iteration, so that at each iteration, current estimates of ψ_{mn} and v_{mn} are available. So at each iteration the task is to find the residuals at each mesh point, and also the partial derivatives of these residuals with respect to the unknowns ψ_{mn} and v_{mn}. We first differentiate the Chebyshev and Fourier series using the appropriate algorithms (e.g., Fox and Parker [13]) and then evaluate ψ, v, and its derivatives on the mesh points. Then the various terms in the ψ equation are found (multiplications being done in the physical space) to obtain the residuals which have to be reduced to zero. Because the only nonlinearities are quadratic, it is straightforward to obtain the partial derivatives of the residuals with respect to the unknowns. This means that the Jacobian matrix required for the Newton–Raphson iteration can be found explicitly, rather than indirectly using numerical differentiation. The advantage of the collocation method is that while the differentiations are done in the function space (where it is simple and accurate), the multiplications are done in the physical space. The procedure for the v equation is similar, except that we set up an $(M-1)\times(N+1)$ mesh on which to calculate the residuals.

A disadvantage of the collocation procedure is that one is restricted to a square truncation scheme such as (3.1); this means that some of the coefficients ψ_{mn} and v_{mn} corresponding to large m and large n are extremely small, and could well be

omitted with considerable saving in time and very little loss of accuracy. We would like to replace (3.1) by

$$\psi = \sum_{n=1}^{N} \sum_{m=0}^{M(n)} \psi_{mn} T_m^*(x) \sin n\alpha\zeta$$
$$v = \sum_{n=0}^{N} \sum_{m=0}^{M(n)} v_{mn} T_m^*(x) \cos n\alpha\zeta \tag{3.2}$$

where $M(n)$ is a decreasing function of n, following the ideas of Clever and Busse [3].

The following definition of $M(n)$ was found to give reasonable results:

$$M(n) = NT + 5 - n, \qquad 0 \leqslant n \leqslant NT - 4,$$
$$M(n) = 9, \qquad NT - 3 \leqslant n \leqslant NT. \tag{3.3}$$

We can no longer simply use the collocation method with this truncation scheme. Fortunately the coefficients are independent of z, and only quadratic nonlinearities are present, so it is not difficult to use a Galerkin procedure in the z-direction. We still use collocation in the x-direction, setting up appropriate meshes on the interval $0 \leqslant x \leqslant 1$, but we do not set up a mesh in the z-direction. Instead the residuals are constructed by equating coefficients of $\sin n\alpha\zeta$ to zero for $1 \leqslant n \leqslant N$. When terms containing products of sines and cosines are encountered, these are expressed as sums of trigonometric functions, e.g., we write $\sin m\alpha\zeta \cos n\alpha\zeta$ as $\frac{1}{2}(\sin(m+n)\,\alpha\zeta + \sin(m-n)\,\alpha\zeta)$. Any term for which $m+n > N$ is ignored. This procedure is more difficult to program than a straightforward collocation procedure, but the final product is slightly better.

With a square truncation, the Jacobian matrix for the Newton–Raphson iteration is of order $(M+1)(2N+1) \times (M+1)(2N+1)$. The maximum truncation parameters, M and N, that are possible are, of course, machine dependent. The calculations reported here were performed on an IBM 370/168 using the FORTRAN H extended optimizing compiler. In order to run sufficiently fast to allow reasonable coverage of the parameter space, we cannot allow the Jacobian matrix to exceed 1 megabyte, with each real taking 8 bytes of storage in double precision. We therefore have an effective constraint of

$$(M+1)(2N+1) \leqslant 362. \tag{3.4}$$

$M = 14$, $N = 11$ or $M = 16$, $N = 10$ were commonly used truncations. The program then takes typically about 5 minutes to obtain an accurately converged Taylor vortex solution.

To evaluate the performance of this technique we tabulate two quantities for a wide range of Taylor numbers and truncation parameters. A natural quantity to examine is the torque of the solutions; on the inner and outer cylinders we have

$$G_{\text{inner}} = G_0 \left[\frac{2(1-\mu)}{\eta(1+\eta)} - \left. \frac{\partial v}{\partial x} \right|_{x=0} \right]; \qquad G_{\text{outer}} = G_0 \left[\frac{2(1-\mu)}{\eta(1+\eta)} - \frac{1}{\eta^2} \left. \frac{\partial v}{\partial x} \right|_{x=1} \right] \tag{3.5}$$

TABLE I

(a)[a]

Ta / $M \times N$	3,500	7,500	15,000	30,000	45,000	60,000	90,000
12 × 4	2.813012	3.5880	4.1788	4.7326			
12 × 6	2.813012	3.5879	4.1860	4.7893	5.1652		
12 × 8	2.813011	3.5879	4.1860	4.7957	5.1911	5.4933	5.9411
12 × 10	2.813012	3.5879	4.1860	4.7959	5.1934	5.5012	5.9710
12 × 12	2.813012	3.5879	4.1860	4.7958	5.1934	5.5019	5.9756
12 × 14	2.813012	3.5879	4.1860	4.7958	5.1934	5.5019	5.9761
8 × 10	2.816624	3.6037	4.2226	4.8774	5.2700	5.5257	
10 × 10	2.813194	3.5859	4.1782	4.7787	5.1670	5.4645	5.9154
12 × 10	2.813012	3.5879	4.1860	4.7959	5.1934	5.5012	5.9710
14 × 10	2.813015	3.5878	4.1866	4.7991	5.1990	5.5087	5.9833
16 × 10	2.813015	3.5878	4.1864	4.7996	5.2009	5.5119	5.9884
16 × 14	2.813015	3.5878	4.1864	4.7996	5.2010	5.5126	5.9940

(b)[b]

12 × 4	4.23304	17.7817	32.3693	51.2371			
12 × 6	4.23355	17.9540	33.4476	54.3842	69.4540		
12 × 8	4.23356	17.9683	33.6420	55.2988	71.2568	84.2016	104.9152
12 × 10	4.23356	17.9693	33.6732	55.5415	71.8396	85.1992	106.8896
12 × 12	4.23356	17.9694	33.6777	55.5996	72.0120	85.5309	107.6370
12 × 14	4.23356	17.9694	33.6783	55.6124	72.0586	85.6325	107.9008
8 × 10	4.27268	18.1675	34.8922	60.9544	84.1644	105.8773	
10 × 10	4.23776	17.9960	33.8165	56.3302	73.8213	88.6912	113.4971
12 × 10	4.23356	17.9693	33.6732	55.5415	71.8396	85.1992	106.8896
14 × 10	4.23363	17.9706	33.6760	55.6582	72.2769	86.1466	109.2237
16 × 10	4.23363	17.9704	33.6752	55.6594	72.2827	86.1107	108.9386
16 × 14	4.23363	17.9705	33.6805	55.7320	72.5085	86.5593	109.9896

[a] The torque, G, is given as a function of Taylor number, Ta, for the case $\eta = 0.5$, $\mu = 0$, $\alpha = 3.1631$. The truncation levels are given as $M \times N$ referring to (3.1).

[b] As above, but tabulating the radial velocity (in the dimensionless units) at the point $z = 0$, $x = \frac{1}{2}$.

where

$$G_0 = \frac{2\pi R_1^3 h \nu \rho \Omega_1}{d},$$

h being the length of the cylinders and ρ the fluid density. In a steady state we should have $G_{\text{inner}} = G_{\text{outer}}$, so any differences are due to truncation error. In Table I, we quote the average value of G_{inner} and G_{outer} as the accepted value (the differences are always very small). Comparison with some of these calculations with previous calculations and fluid experiments is given in Jones [17]. The torque,

being an averaged quantity over the dominant modes, is not a very stringent test of the accuracy of the solutions, so we also quote the radial velocity at the point $z=0$, $x=\frac{1}{2}$ in Table I. This point is situated between adjacent toroidal cells; the radial velocity is nearly a maximum at this location.

It can be seen from Table I that for low Ta ($Ta_{\text{crit}} \cong 3099$) both the given quantities converge very rapidly with M and N, as we expect with fully spectral methods. It is also clear that significant errors are occurring at the higher values of Ta, indicating the increased resolution requirement at higher Ta. It would be of some interest to know how rapidly M and N must increase with Ta in order to maintain constant accuracy. Unfortunately, to get a definitive answer to this requires computation at large Ta (to get to the asymptotic regime) and with larger M and N than the resources available here permit. However, the following argument is consistent with the data given in Table I. In the x-direction, the boundary layer scales as $\delta \sim Ta^{-1/4}$. The intervals between zeros of the Chebyshev polynomials scale with M^{-2} in these boundary layers, so to maintain constant resolution we need $M \sim Ta^{1/8}$. In the z-direction we have internal boundary layers between the vortices, again with $\delta \sim Ta^{-1/4}$. The periodic functions used to represent the z-dependence have zeros which are uniformly spaced, so to maintain resolution in the internal boundary layers we need $N \sim Ta^{1/4}$. The scaling $N \sim Ta^{1/4}$ fits the Table I data quite nicely. The $M \sim Ta^{1/8}$ law is not so clear (a power between $\frac{1}{8}$ and $\frac{1}{4}$ gives a better fit), but this may be simply because we are not yet in the asymptotic regime. The relative errors in the eigenvalues due to the $M \times N$ truncation are given in Section 5.

4. Methods Used for the Stability Equations

(a) *The SS Method*

We now consider methods for solving (2.11) and (2.12), where the axisymmetric velocity fields $\mathbf{u}^0$ have now been found numerically, and are available in a convenient form, such as a Chebyshev and Fourier representation. For a fully spectral method, the representation (2.13) is convenient. We write, for out-of-phase modes,

$$\begin{aligned} \theta &= \sum_{n=0}^{N} \sum_{i=0}^{M} \theta_{in} T_i^*(x) \cos n\alpha\zeta \, e^{im\phi} e^{i\omega t + \sigma t} \\ \chi &= \sum_{n=1}^{N} \sum_{i=0}^{M} \chi_{in} T_i^*(x) \sin n\alpha\zeta \, e^{im\phi} e^{i\omega t + \sigma t}. \end{aligned} \tag{4.1}$$

In-phase modes (see [17]) can be treated similarly. The boundary conditions give $4N$ equations on χ and $2(N+1)$ equations on θ. As with the axisymmetric equations we use collocation in the x-direction and the Galerkin procedure in the z-direction. Thus, inserting the expression (4.1) into Eqs. (1.13), (2.11), and (2.12) results in $N(M-3)+(N+1)(M-1)$ equations of the form

$$(\sigma + i\omega)\, \mathbf{L}_1 \mathbf{a} = \mathbf{L}_2 \mathbf{a} \tag{4.2}$$

where the single vector **a** is made up by running the unknown θ_{in} and χ_{in} together. At this stage, we still have $N(M+1)+(N+1)(M+1)$ unknowns, so we use the boundary conditions to eliminate the elements of **a** corresponding to $\chi_{M-3,n}$, $\chi_{M-2,n}$, $\chi_{M-1,n}$, $\chi_{M,n}$ for $n=1, N$ and $\theta_{M-1,n}$, $\theta_{M,n}$ for $n=0, N$. Then (4.2) is reduced to a square system in which $\mathbf{L}_1$ is a nonsingular matrix. Equation (4.2) was solved by inverting $\mathbf{L}_1$ and finding $\mathbf{L}_1^{-1}\mathbf{L}_2$, and then using a standard package (routine F02AJF of the Numerical Algorithm Group Library) which reduces $\mathbf{L}_1^{-1}\mathbf{L}_2$ to Hessenberg form and then applies the LR algorithm (see, e.g., Wilkinson [33]) to find all the eigenvalues. The matrix $\mathbf{L}_2$ is a dense, complex matrix. $\mathbf{L}_1$ is block diagonal with $2N\times 2N$ blocks. Storage (and time) restrictions are therefore tighter on the stability equations than they are on the axisymmetric program. With each element of the matrices requiring 16 bytes, the 1-megabyte limit is now the constraint

$$(M+1)(2N+1)\leqslant 256 \tag{4.3}$$

and in practice values of $M\times N$ of 12×9 or 11×10 were possible. For Taylor numbers $\leqslant 5Ta_c$ more rectangular truncations, such as $M=14$, $N=6$, gave better results. Details are given in Section 5, Table II.

The computational time for the SS method is $\sim M^3N^3$ as M and N become large. This asymptotic behaviour would hold, even if a different method, such as inverse iteration, were used to find the eigenvalues.

(b) *The SF Method*

As can be seen from Table II, the results of the SS method become insufficiently accurate to determine the stability boundary reliably for $Ta\gtrsim 24{,}000$ at $\eta=0.77$. As there are a number of interesting experiments on the onset of wavy vortices in long Taylor apparatuses conducted at $Ta>24{,}000$ (e.g., Cole [4], Park [28], Lorenzen, Pfister, and Mullin [20]) it is of interest to develop methods for finding the eigenvalues at higher Taylor numbers.

Any effective method based on a local approximation, such as finite differences, must take advantage of the sparsity pattern of the associated matrices. There are two reasons why this is particularly true for this type of problem: firstly, the high differential order (sixth) naturally favours global methods, where differentiation is easy and accurate, to local methods such as finite differences. Secondly, the well-known rapid convergence properties of Chebyshev polynomials (and Fourier representation for periodic functions) means that considerably more mesh points are needed than expansion functions.

At Taylor numbers of the order of 50,000 more than twice as many mesh points were required in the z-direction as Fourier modes in z to achieve comparable accuracy, even though a fourth-order-accurate method was used. Our experience also indicates that the same is true in the radial direction, i.e., more than twice as many mesh points are needed as Chebyshev polynomials. In consequence, it required a considerable amount of program development before any method

involving finite differences was found that was superior to the SS method described in Section 4(a).

Several FF methods were tried, but none proved to be competitive with the SF method described below. The formulation used for these attempts was that of the three coupled Poisson-type equations (2.15) to (2.17), and the method adopted was inverse iteration. The complex matrix equations which have to be solved are closely coupled in the three variables, and are highly asymmetric. It is believed that this is the reason why the iteration methods used to solve the matrix equations failed to converge satisfactorily. Direct methods of solution did produce results, but none of the methods tried led to an FF method that was competitive with the SF method described below. Two direct methods were considered for solving the FF equations, the variable band method (Jennings [15], Duff [9]) and the use of the Markowitz pivoting strategy with indirect addressing (e.g., Duff [9]). The variable band method takes advantage of the sparseness induced by the local approximation in one direction, but not in the second direction. Infill of zeros occurs as the elimination proceeds. The use of a pivoting strategy is designed to counteract this problem, and it would probably be superior in the limit of very large numbers of mesh points. However, for this problem (mainly due to the complicated nature of the equations) the overheads incurred by the indirect addressing mean that the pivoting strategy would not show its superiority until the mesh size was about 40×40 by which size the CPU time consumed is unacceptably large. It should also be noted that the indirect addressing required by the pivotal strategy makes it less attractive for use on a machine with vector capabilities.

Since the variable band method was found to be the most advantageous method of solving the FF equations, there is no longer any point in using a local rather than a global approximation in one direction; if the zeros are going to be filled in, we may as well replace them by nonzeros which greatly improve the accuracy of the results! So we are naturally led to using SF methods.

In the SF method selected, we represented the axial direction by finite differences and the radial direction by Chebyshev polynomials. The decision to use the finite differences in the z-direction, rather than in the r-direction, was motivated by the need to examine disturbances which have an axial wavelength longer than the axial wavelength of the axisymmetric vortices; these disturbances are important for some radius ratios (Jones [16], Cole [4]). Modes of this type have a higher effective resolution requirement in the z-direction; since computational cost varies only linearly with the number of points in the z-direction, it is better to put the mesh points in the direction which has the most demanding resolution requirement. An approximation to the desired eigenvalue at any given Taylor number is available either from a previous run at a lower Taylor number or from the method described in Section 4(a). Since the eigenvalues are well spaced out in the complex plane (we know this from our studies with the SS method, where the LR algorithm finds all the eigenvalues of the matrix), inverse iteration is an appropriate method to find the eigenvalues. We represent

$$u_r^{(j)} = \sum_{i=0}^{M} U_{ij} T_i^*(x)$$

$$u_z^{(j)} = \sum_{i=0}^{M} W_{ij} T_i^*(x) \tag{4.4}$$

$$p^{(j)} = \sum_{i=0}^{M} P_{ij} T_i^*(x)$$

where $u_r^{(j)}$, $u_z^{(j)}$, and $p^{(j)}$ are the values of u_r, u_z, and p at the jth mesh point in the ζ-direction. We substitute these expressions into Eqs. (2.15) to (2.17). All differentiating in the x-direction is then done as usual directly on the Chebyshev series: derivatives in the z-direction are represented by second-order centred finite differences, so $\partial U_i/\partial z|_{z=z_j}$ is represented by $(U_{i,j+1} - U_{i,j-1})/2\delta z$ and $\partial^2 U_i/\partial z^2|_{z=z_j}$ by $(U_{i,j+1} - 2U_{i,j} + U_{i,j-1})/\delta z^2$, etc. The Chebyshev series are evaluated on mesh points in the x-direction corresponding to the zeros of the appropriate Chebyshev polynomial. The condition that the equations be satisfied exactly at these mesh points leads to linear simultaneous equations of the form

$$\mathbf{A}_1 \mathbf{x} = (\sigma + i\omega)\, \mathbf{B}_1 \mathbf{x} \tag{4.5}$$

from Eqs. (2.16) and (2.17), and equations of the form

$$\mathbf{A}_2 \mathbf{x} = \mathbf{0} \tag{4.6}$$

from (2.15) and from the boundary conditions. Here $\mathbf{x}$ is a vector whose components are made up of running the coefficients U_{ij}, W_{ij}, and P_{ij} together. Since (4.5) and (4.6) must be solved simultaneously we run the matrices $\mathbf{A}_1$ and $\mathbf{A}_2$ together to obtain the eigenvalue problem

$$\mathbf{A}^{(2)} \mathbf{x} = \lambda \mathbf{B} \mathbf{x}. \tag{4.7}$$

Here $\mathbf{B}$ is singular; it has been constructed by adding an appropriate number of zeros to $\mathbf{B}_1$; the superscript 2 on the matrix $\mathbf{A}$ denotes that it has been derived using second-order finite differences.

For out-of-phase modes, $u_r = p = 0$ at $\zeta = 0$, so if the mesh points in the z-direction run from 1 to N (corresponding to $\zeta = 0$ and $\zeta = \pi/\alpha$, respectively), then $U_{i1} = U_{iN} = P_{i1} = P_{iN} = 0$ for all $i = 0, M$. We use Eq. (2.17) to derive an equation determining W_{ij} on the $\zeta = 0$ and $\zeta = 2\pi/\alpha$ boundaries; from the periodicity, we can set $\partial P_{i1}/\partial z = (P_{i2} - P_{i0})/2\delta z = P_{i2}/\delta z$: other derivatives are treated similarly. So $\mathbf{A}^{(2)}$ is a square matrix of order $(M+1) \times (3N-4)$ by $(M+1) \times (3N-4)$. We order the U_{ij}, W_{ij}, and P_{ij} inside $\mathbf{x}$ in such a way that the matrix $\mathbf{A}^{(2)}$ has the block form of Fig. 1, where each block a_{ij} is a dense square block of size $(3M+3) \times (3M+3)$, except for the end blocks, which are smaller.

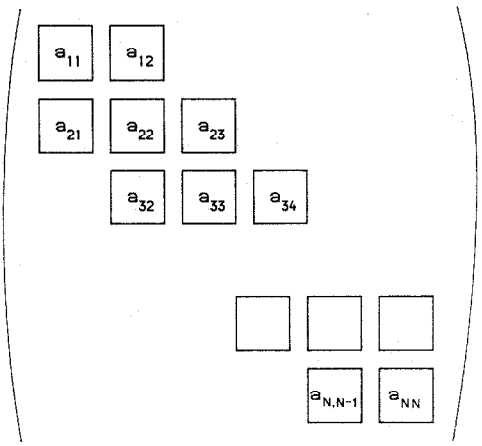

FIGURE 1

In the inverse iteration method, we choose an initial guess for the eigenvalue, $\sigma_0 + i\omega_0 = \lambda_0$, and perform the following iteration scheme:

$$(\mathbf{A}^{(2)} - \lambda_0 \mathbf{B})\, \mathbf{y}^{i+1} = \mathbf{B}\mathbf{x}^i; \qquad \mathbf{x}^{i+1} = \mathbf{y}^{i+1}/\|\mathbf{y}^{i+1}\|. \tag{4.8}$$

The normalisation is not very important; for the work described here, the coefficient of $T_2^*(x)$, in u_z evaluated at $\zeta = 0$, was set to 1. This coefficient is always comparatively large for a wavy mode. We also chose an initial guess, $\mathbf{x}^0$; again, this choice is not very crucial; it is, however, important to make λ_0 as good an estimate for the eigenvalue as possible. As $i \to \infty$, $\mathbf{x}^i$ converges towards that eigenvector whose eigenvalue λ gives $|\lambda - \lambda_0|$ the smallest value. Further, $x_m^{i+1}/y_m^{i+1} \to r$, a complex constant, and the eigenvalue corresponding to the converged eigenvector is given by $\lambda = \lambda_0 + r$. No difficulties are caused by $\mathbf{A}^{(2)} - \lambda_0 \mathbf{B}$ being nearly singular if λ_0 is an accurate guess. The matrix $\mathbf{A}^{(2)} - \lambda_0 \mathbf{B}$ has a structure as in Fig. 1. In order to perform the iteration scheme (4.8) we need to decompose $\mathbf{A}^{(2)} - \lambda_0 \mathbf{B}$ into LU form by Gaussian elimination.

The algorithm used for this decomposition was as follows: at the ith stage, block $a_{i,i-1}$ has been reduced to zero, so we eliminate $a_{i+1,i}$ and the lower triangle of $a_{i+1,i+1}$ using as pivots elements from the block a_{ii}. This involves subtracting elements of $a_{i,i+1}$ from elements of $a_{i+1,i+1}$. It was found not to be necessary to choose pivots from block $a_{i,i+1}$. At each stage in the elimination, the pivot element chosen was that element of largest modulus in the appropriate row in block a_{ii}. All calculations were done in double precision complex arithmetic. As each block is completed, the triangularised a_{ii} and the still square $a_{i,i+1}$ are passed out of main core storage, and the next blocks brought in so the total amount of core storage required is governed by the size of each block, and not by the size of the whole matrix $\mathbf{A}^{(2)}$. This method of elimination is sometimes referred to as the "frontal" method (e.g., Duff [9]).

The LU decomposition is the most time-consuming part of the program to find the eigenvalue, even though it is only done once: the operation count is proportional to M^3N for large M and N. This compares with M^3N^3 for the SS method described in Section 4(a). It should be noted that no indirect addressing is required for the inner loop of the elimination procedure, so the algorithm is likely to be particularly suitable for a machine with vector capabilities, although all the

been done, it is merely a matter of back-substitution to perform the iteration (4.8), even from a rather arbitrary initial guess for $\mathbf{x}^0$, eight iterations are usually sufficient to obtain a well-converged solution; the eigenvalues are well spread out in this problem. Each iteration requires the decomposed form of $\mathbf{A}^{(2)}-\lambda_0\mathbf{B}$ to be brought in and out of main core storage: the operation count here is proportional to M^2N, but nevertheless this is a potential bottleneck. However, on the IBM 370/168 the LU description took about three times as much time as doing eight iterations with the decomposed form for the values of $M=16$ and $N=41$ which were used for many of the runs.

The eigenvalue, λ, obtained by this method is only accurate to second order in δz, because $\mathbf{A}^{(2)}$ has been obtained by second-order finite differences. We could construct $\mathbf{A}^{(4)}$, the matrix corresponding to using the fourth-order centred difference approximations

$$\left.\frac{dy}{dz}\right|_{z=0}=\frac{y_1-y_{-1}}{2\delta z}-\frac{1}{12\delta z}(y_2-2y_1+2y_{-1}-y_{-2})+O(\delta z^4)$$
$$\left.\frac{d^2y}{dz^2}\right|_{z=0}=\frac{y_1-2y_0+y_{-1}}{\delta z^2}-\frac{1}{12\delta z^2}(y_2-4y_1+6y_0-4y_{-1}+y_{-2})+O(\delta z^4). \tag{4.9}$$

If we did this, the form of Fig. 1 would be changed to having five blocks in each row instead of three, with a considerable increase in the work required to do the LU decomposition. It is, however, possible to find the eigenvalue so that the error is $O(\delta z^4)$ without doing any LU decomposition other than the decomposition of $\mathbf{A}^{(2)}-\lambda_0\mathbf{B}$. This is done by using perturbation theory based on the assumption that the second-order eigenvectors are reasonably close to the true eigenvectors. We let

$$\mathbf{A}^{(4)}=\mathbf{A}^{(2)}+\mathbf{A}^{(c)} \tag{4.10}$$

so that $\mathbf{A}^{(c)}$ is a correction matrix. If we proceeded to solve the fourth-order problem directly, we would end up with a fourth-order eigenvector $\mathbf{x}^{(2)}+\mathbf{x}^{(c)}$ satisfying

$$[\mathbf{A}^{(2)}+\mathbf{A}^{(c)}-\lambda_0\mathbf{B}](\mathbf{x}^{(2)}+\mathbf{x}^{(c)})=(r^{(2)}+r^{(c)})\,\mathbf{B}(\mathbf{x}^{(2)}+\mathbf{x}^{(c)}). \tag{4.11}$$

The essential step in the method is to ignore the terms $\mathbf{A}^{(c)}\mathbf{x}^{(c)}$ and $r^{(c)}\mathbf{B}\mathbf{x}^{(c)}$ in (4.11), which are $O(\delta z^4)$, in comparison with the other terms involving corrections, which are $O(\delta z^2)$. We start by solving the second-order problem as above, so we

have an LU decomposition $\mathbf{A}^{(2)} - \lambda_0 \mathbf{B}$, and an eigenvector $\mathbf{x}^{(2)}$ and eigenvalue $\lambda_0 + r^{(2)}$. So

$$(\mathbf{A}^{(2)} - \lambda_0 \mathbf{B})\, \mathbf{x}^{(2)} = r^{(2)} \mathbf{B} \mathbf{x}^{(2)}. \tag{4.12}$$

Since we have the LU decomposition of $\mathbf{A}^{(2)} - \lambda_0 \mathbf{B} \equiv \mathbf{LU}$, we can solve for the adjoint eigenvector $\mathbf{y}^{(2)}$ by means of the inverse iteration procedure

$$\mathbf{z}^{i+1} \mathbf{LU} = \mathbf{y}^i \mathbf{B}; \qquad \mathbf{y}^{i+1} = \mathbf{z}^{i+1} / \|\mathbf{z}^{i+1}\| \tag{4.13}$$

so that the adjoint $\mathbf{y}^{(2)}$ satisfies

$$\mathbf{y}^{(2)} (\mathbf{A}^{(2)} - \lambda_0 \mathbf{B}) = r^{(2)} \mathbf{y}^{(2)} \mathbf{B}. \tag{4.14}$$

Finding the adjoint requires only back-substitutions, and not a new LU decomposition: the work required is therefore asymptotically $O(M^2 N)$. The eigenvalue obtained from the adjoint problem is the same as that obtained by the original problem (which provides a useful numerical check), although the eigenvector $\mathbf{y}^{(2)}$ is quite different from $\mathbf{x}^{(2)}$. We now use the identity

$$\mathbf{y}^{(2)} [\mathbf{A}^{(2)} + \mathbf{A}^{(c)} - \lambda_0 \mathbf{B}] (\mathbf{x}^{(2)} + \mathbf{x}^{(c)}) = \mathbf{y}^{(2)} (r^{(2)} + r^{(c)})\, \mathbf{B} (\mathbf{x}^{(2)} + \mathbf{x}^{(c)}) \tag{4.15}$$

which, using (4.12) and (4.14), reduces to

$$\mathbf{y}^2 \mathbf{A}^{(c)} \mathbf{x}^{(2)} + \mathbf{y}^{(2)} \mathbf{A}^{(c)} \mathbf{x}^{(c)} = r^{(c)} \mathbf{y}^{(2)} \mathbf{B} \mathbf{x}^{(2)} + \mathbf{y}^{(2)} r^{(c)} \mathbf{B} \mathbf{x}^{(c)}. \tag{4.16}$$

Neglecting $\mathbf{x}^{(c)}$ compared to $\mathbf{x}^{(2)}$ (in the limit $\delta z \to 0$ it is $O(\delta z^2)$ smaller),

$$r^{(c)} = \frac{\mathbf{y}^{(2)} \mathbf{A}^{(c)} \mathbf{x}^{(2)}}{\mathbf{y}^{(2)} \mathbf{B} \mathbf{x}^{(2)}} + O(\delta z^4) \tag{4.17}$$

so that $\lambda = \lambda_0 + r^{(2)} + r^{(c)}$ is an eigenvalue with error only $O(\delta z^4)$. Since the work done to calculate (4.17) is comparatively small, the only significant extra work done is the calculation of $\mathbf{y}^{(2)}$, via (4.13). The time taken for this is approximately the same as for the iteration scheme (4.8), which is typically only one-third the time taken to perform the LU decomposition. We thus obtain a considerable improvement in the accuracy of the eigenvalue at comparatively little computational cost.

5. Performance of the Algorithms for the Stability Problem

The quantities that are usually measured in fluid experiments are the critical Taylor number, *Ta*, for the onset of unstable waves (where the real part of $\lambda = 0$) and the wave frequency at onset. The accuracy with which these can be determined numerically depends on how accurately we can measure the eigenvalue, so we concentrate on this quantity. The form of the eigenfunctions is of interest, but to date

TABLE II[a]

Ta	η	M	N	σ	ω
12,000	0.78	12	9	−0.25	−59.51
12,000	0.78	14	7	−0.36	−59.68
12,000	0.78	15	6	−0.56	−59.53
12,000	0.78	11	10	−0.27	−59.60
24,000	0.77	14	7	−0.53	−78.21
24,000	0.77	15	6	1.09	−77.46
24,000	0.77	12	9	0.47	−77.45
24,000	0.77	11	10	0.23	−79.15

[a] The eigenvalue, $\sigma + i\omega$, is given for various truncations at the two points $Ta = 12{,}000$, $\eta = 0.78$, $\alpha = 3.13$, $\mu = 0$ and $Ta = 24{,}000$, $\eta = 0.77$, $\alpha = 3.13$, and $\mu = 0$.

the comparison here with observations is only qualitative, so the need for high-accuracy eigenfunctions is not so pressing. We therefore concentrate in this section on the accuracy of the eigenvalues. In addition to quoting the wave frequency measured on the viscous time scale, we also give the dimensionless phase speed, P.S. $= \omega/m\Omega_1$. When the gap between the cylinders is narrow, this is close to $\frac{1}{2}$, but in wide-gap cases the phase speed can fall well below this value.

The purpose of this section is to estimate the errors incurred by truncating the

TABLE III[a]

$M \times N$	NX	NZ	$\sigma^{(4)}$	$\omega^{(4)}$	$\sigma^{(2)}$	$\omega^{(2)}$	P.S.
16 × 10	12	25	0.363	−77.764	0.374	−75.938	0.2856
16 × 10	12	33	0.401	−77.907	0.377	−76.798	0.2861
16 × 10	12	41	0.415	−77.953	0.388	−77.214	0.2863
16 × 10	14	25	0.443	−77.757	0.421	−75.919	0.2855
16 × 10	14	33	0.487	−77.891	0.441	−76.782	0.2860
16 × 10	14	41	0.504	−77.934	0.460	−77.197	0.2862
16 × 10	16	25	0.425	−77.756	0.407	−75.917	0.2855
16 × 10	16	33	0.468	−77.890	0.424	−76.780	0.2860
16 × 10	16	41	0.484	−77.933	0.443	−77.196	0.2862
14 × 11	16	41	0.492	−77.927	0.452	−77.190	0.2862
$NT = 13$	16	41	0.476	−77.934	0.436	−77.197	0.2862
$NT = 12$	16	41	0.485	−77.930	0.443	−77.194	0.2862
16 × 10	12	EXT	0.428	−77.989	0.431	−77.998	0.2863
16 × 10	14	EXT	0.518	−77.967	0.522	−77.975	0.2863
16 × 10	16	EXT	0.498	−77.966	0.502	−77.975	0.2863

[a] All calculations have $Ta = 24000$, $\eta = 0.77$, $\alpha = 3.13$, $\mu = 0$, and $m = 3$. $\lambda^{(4)} = \sigma^{(4)} + i\omega^{(4)}$ is the computed eigenvalue with the fourth-order correction. $\lambda^{(2)} = \sigma^{(2)} + i\omega^{(2)}$ is the computed eigenvalue without the correction. EXT means the value obtained by Richardson extrapolation; $NT = 13$ refers to the truncation scheme (3.3).

TABLE IV[a]

$M \times N$	NX	NZ	m	$\sigma^{(4)}$	$\omega^{(4)}$	P.S.
16×10	12	41	3	0.56	−105.18	0.2417
16×10	13	41	3	0.41	−105.06	0.2414
16×10	14	41	3	0.51	−105.04	0.2414
16×10	15	41	3	0.60	−105.07	0.2415
16×10	16	41	3	0.59	−105.11	0.2416
16×10	16	33	3	0.57	−105.02	0.2414
16×10	16	25	3	0.53	−104.73	0.2407
14×11	16	41	3	0.47	−105.04	0.2414
$NT = 13$	16	41	3	0.43	−105.10	0.2415
$NT = 12$	16	41	3	0.64	−105.10	0.2415
16×10	16	EXT	3	0.62	−105.19	0.2418
16×10	15	49	1	−2.72	−33.41	0.2306
16×10	15	60	1	−2.82	−33.46	0.2307
16×10	16	49	1	−2.76	−33.40	0.2303
16×10	16	60	1	−2.85	−33.45	0.2306
16×10	16	EXT	1	−2.93	−33.48	0.2309
14×11	16	60	1	−3.03	−33.60	0.2316
$NT = 13$	16	60	1	−3.05	−33.67	0.2321
$NT = 12$	16	60	1	−2.75	−33.38	0.2301

[a] All calculations have $Ta = 48{,}000$, $\eta = 0.73$, $\alpha = 3.13$, $\mu = 0$. $\lambda^{(4)} = \sigma^{(4)} + i\omega^{(4)}$ is the eigenvalue with the fourth-order correction. EXT means the value obtained by Richardson extrapolation; $NT = 13$ refers to the truncation scheme (3.3).

TABLE V[a]

$M \times N$	NX	NZ	m	$\sigma^{(4)}$	$\omega^{(4)}$	P.S.
16×10	12	41	3	1.13	−142.42	0.2185
16×10	13	41	3	0.52	−143.40	0.2200
16×10	14	41	3	0.14	−144.18	0.2212
16×10	15	41	3	0.18	−143.63	0.2203
16×10	16	41	3	0.43	−143.65	0.2204
16×10	17	41	3	0.42	−143.81	0.2206
16×10	18	41	3	0.43	−143.85	0.2207
16×10	16	33	3	0.37	−143.39	0.2200
16×10	16	25	3	0.25	−142.63	0.2185
16×10	16	EXT	3	0.48	−143.87	0.2207
14×11	16	41	3	−0.72	−142.19	0.2181
$NT \times 13$	16	41	3	−0.52	−142.68	0.2189
$NT \times 12$	16	41	3	0.02	−143.20	0.2197

[a] All calculations have $Ta = 96{,}000$, $\eta = 0.71$, $\alpha = 3.13$, $\mu = 0$. $\lambda^{(4)} = \sigma^{(4)} + i\omega^{(4)}$ is the eigenvalue with the fourth-order correction. EXT means the value obtained by Richardson extrapolation; $NT = 13$ refers to the truncation scheme (3.3).

TABLE VI[a]

Ta	m	η	σ	ω	Error
24,000	3	0.77	0.498	−77.968	±0.005
48,000	3	0.73	0.57	−105.14	±0.03
48,000	1	0.73	−3.04	−33.61	±0.05
96,000	3	0.71	−0.06	−143.22	±0.10

[a] Best estimates for the eigenvalues at selected points with $\alpha = 3.13$ and $\mu = 0$. The error estimate refers to both σ and ω.

infinite expansions, and to give high-accuracy eigenvalues for a small number of selected points. A much fuller coverage of the parameter space is given in [16]. As test points we have chosen values of Ta and η near the stability boundary, with a large variation in Ta. In Table II we give results from the SS method described in Section 4(a). In Tables III, IV, and V we give results derived from the SF method discussed in Section 4(b). These results are based on a number of different truncations, allowing us to estimate errors. In Table VI we give the best estimates and probable errors for a few particular cases to help calibrate other programs. For this purpose the constraint (4.3) has been relaxed.

The first of the two points examined with the fully spectral SS method is at $Ta = 12{,}000$, $\eta = 0.78$, $\alpha = 3.13$, and $\mu = 0$. The disturbance examined is $m = 3$, which is the most unstable at these parameter values. This is also true for the second point examined, at $Ta = 24{,}000$, $\eta = 0.77$, $\alpha = 3.13$, and $\mu = 0$. The results are listed in Table II. Truncation errors in the real and imaginary parts of the eigenvalue are of similar absolute magnitude. Given the constraint (4.3), set by storage and time considerations, to estimate errors we find the value of λ on the basis of a number, n, of different truncations and look at the dispersion

$$S = \left[\frac{1}{n}\sum_{i=1}^{n} |\lambda_i - \lambda_m|^2\right]^{1/2} \tag{5.1}$$

where λ_m is the mean of the calculated eigenvalues. Applying this to the values found in Table II, we find that for the point at $Ta = 12{,}000$, $\lambda_m = -0.36 - 59.58i$ and S is 0.14; at $Ta = 24{,}000$, $\lambda_m = 0.31 - 78.07i$ and $S = 0.90$. These results are consistent with the eigenvalues computed by the more accurate SF method described in Section 4(b), if we interpret the dispersion, S, as the estimated truncation error. Note that the dispersion, S, has increased very substantially with Ta. Although the boundary layer arguments at the end of Section 3 indicated that the number of expansion functions required to maintain constant accuracy increases at a comparatively modest rate, the fast rate of convergence of the Chebyshev and Fourier series means that S is a very sensitive function of M and N. In consequence, where the constraint (4.3) is operative, the dispersion, S, is a rapidly increasing function of Ta. If we wish to keep S constant, we need $N \sim Ta^{1/4}$ and $M \sim Ta^{1/8}$; with computational time

increasing as M^3N^3, to keep S constant computational time must increase as $Ta^{9/8}$ or $Re^{9/4}$.

It is of interest to know what errors are likely to occur in Ta_w as a result of errors in the eigenvalue. This depends on the values of $(1/Ta)(\partial Ta/\partial\sigma)$. At the points in the tables corresponding to 24,000, 48,000, and 96,000, $(1/Ta)(\partial Ta/\partial\sigma)$ is approximately 0.46, 0.37, and 0.63, respectively. But away from $\eta \cong 0.75$ the values of $(1/Ta)(\partial Ta/\partial\sigma)$ are generally considerably smaller.

For the SF method of Section 4(b) we can identify three distinct sources of truncation error. First, the finite truncation $M \times N$ used in the axisymmetric Taylor vortex calculation; second, the finite number of Chebyshev polynomials in the radial direction, NX; and, third, the finite number of mesh points used in the z-direction. To avoid confusion with the truncation parameters for the axisymmetric problem, we denote the truncation parameter for the Chebyshev polynomials by NX (so number of polynomials used is $NX+1$) and the number of mesh points by NZ. In Tables III, IV, and V we have varied each of these three factors separately in order to estimate the scatter as the truncation parameters are varied, and hence estimate the errors in the eigenvalues.

To investigate the errors due to finite NZ, we keep $M \times N$ and NX constant, and vary only NZ. The results of these tests show that the fourth-order corrections give a substantially more accurate eigenvalue than the uncorrected second-order results. To achieve full fourth-order convergence, however, we need NZ greater than 41; the results from Tables III, IV, and V indicate a rate of convergence nearer h^3 than h^4. Full fourth-order convergence can be obtained at values of the Taylor number lower than 24,000 with values of NZ around 41 or by increasing NZ at the higher Taylor numbers. We also include in Tables III, IV, and V the results of Richardson extrapolation based on fourth-order extrapolation of the $NZ=33$ and 41 pair. When investigating the parameter space, it is not practical to perform Richardson extrapolation at every point, so we have also investigated the errors incurred by leaving NZ constant at 41.

The errors due to finite NX fall off very rapidly as NX increases, but they are not amenable to Richardson extrapolation. The best we can do is to vary NX and estimate the variation in the eigenvalue. Similar considerations apply to the errors measured by having finite $M \times N$. We note that here we have a constraint such as (3.4) to contend with.

The results in Table III are consistent with fourth-order convergence for the corrected eigenvalues $\lambda^{(4)} = \sigma^{(4)} + i\omega^{(4)}$ and second-order convergence for the uncorrected eigenvalues $\lambda^{(2)} = \sigma^{(2)} + i\omega^{(2)}$. Similar behaviour holds for the other points tested. At $Ta = 24{,}000$, if we hold NX and NZ constant at 16 and 41, the scatter over the four Taylor vortex truncations is 0.006. At $Ta = 48{,}000$ this has risen to 0.09 and at $Ta = 96{,}000$ it is 0.7. As we might expect, the increase in the error is as steep as in the SS eigenvalue method of Section 4(a). The error due to the NX truncation is about 0.02 at $Ta = 24{,}000$, 0.05 at $Ta = 48{,}000$, and about 0.2 at $Ta = 96{,}000$ when $NX = 16$. With $NZ = 41$, the error due to finite NZ is about 0.03 at $Ta = 24{,}000$, 0.109 at $Ta = 48{,}000$, and 0.25 at $Ta = 96{,}000$.

The $m = 1$ mode results in Table IV show that this mode is more difficult to find accurately than the $m = 3$ mode: in particular it requires greater resolution in the z-direction. The corresponding errors are therefore somewhat greater.

In Table VI we give the best estimates of the eigenvalues for the cases examined here, together with estimates of the errors. In deriving these results we have abandoned the storage constraint (4.3). Values of $M \times N$ up to 16×14 have been used, with NX up to 16 and NZ extrapolated to infinity.

The typical CPU time taken on the 370/168 to find the axisymmetric Taylor vortices with $M \times N$ at 16×10 was about 5 minutes; for the perturbations with $NX \times NZ = 16 \times 41$ the typical time was about 7 minutes. At $NX = 16$, this time increased slightly less rapidly than NX^3, the theoretical asymptotic value as $NX \to \infty$. The time is linear with NZ. As is indicated by these figures, the principal source of error for $Ta \geq 40{,}000$ is in the axisymmetric Taylor vortex calculation. Because of its poor asymptotic behaviour, this becomes increasingly true as the Taylor number increases. We note, by comparison with Table I, that the relative errors in the eigenvalues are considerably higher than those in the torque, which is known to be a relatively insensitive measure of the accuracy of a Taylor vortex program (Rogers and Beard [31]). However, the present programs can find eigenvalues to about 1% accuracy up to $Ta \cong 100{,}000$, and to better than 0.1% accuracy for $Ta \leq 25{,}000$ within the stated machine resources.

6. Conclusions

For low Taylor numbers ($Ta \leq 5Ta_{\text{crit}}$) the fully spectral methods (SS type) are undoubtedly superior to any other method known to the author for this type of problem, when there are neither boundary layers nor singularities in the flow. This applies to axisymmetric nonlinear calculations of Taylor vortex flow and especially to the resolution of the stability problem, where the fully spectral methods give a lot of information relatively cheaply. However, as the Taylor number increases, and finer structures develop in the flow, the fully spectral methods begin to lose their great advantage. Although the number of spectral functions required increases less rapidly than the number of finite difference points as the Taylor number increases, this is more than outweighed by the penalty incurred by inverting full matrices rather than sparse matrices. On the other hand, using finite difference methods in both directions is not effective for this problem, as the price paid to ensure numerical stability is too great: we found here that a mixed spectral-finite difference approach gave the best results at high Taylor number.

For the methods described in Section 4, the break-even point between fully spectral and mixed SF methods was at about $Ta \sim 10Ta_{\text{crit}}$. However, this break-even point is dependent on both the budget available and the accuracy required. Some indication of the budget and accuracy used for this study can be obtained from Section 5. At given Taylor number spectral methods have superior convergence properties to finite difference methods. In consequence, if higher accuracy is demanded

(and a higher budget allowed) fully spectral methods will be favoured, and the break-even point will rise somewhat above $10Ta_{crit}$.

In order to get high-accuracy eigenvalues it is necessary to have very high accuracy axisymmetric Taylor vortices to perturb. The results indicate that the main source of error in the eigenvalues is now in this nonlinear calculation when the SF method is used for the stability. However, the use of the methods described here greatly extends the range of parameter space compared to that which can be covered using the traditional fully spectral methods.

REFERENCES

1. G. K. BATCHELOR, *J. Fluid Mech.* 7 (1960), 416–418.
2. O. BOOZ, "Numerische Losung der Navier–Stokes–Gleichungen für Taylor–Wirbelströmungen im weiten Spalt," Ph.D. thesis, Stuttgart University, 1980.
3. R. M. CLEVER AND F. H. BUSSE, *J. Fluid Mech.* **65** (1974), 625–645.
4. J. A. COLE, The effect of cylinder radius ratio on wavy vortex onset, *in* "Proceedings, 3rd Taylor-Vortex Working Party Meeting, at Nancy, 1983."
5. A. DAVEY, *J. Fluid Mech.* **14** (1962), 336–368.
6. A. DAVEY, R. C. DIPRIMA, AND J. T. STUART, *J. Fluid Mech.* **31** (1968), 17–52.
7. R. C. DIPRIMA AND H. L. SWINNEY, Instabilities and transition in flow between concentric rotating cylinders, *in* "Hydrodynamic Instabilities and the Transition to Turbulence" (H. L. Swinney and J. P. Gollub, Eds.), pp. 139–180, Springer-Verlag, New York/Berlin, 1981.
8. I. S. DUFF AND J. K. REID, "Experience of Sparse Matrix Codes on the CRAY-1," AERE Harwell report, 1981.
9. I. S. DUFF, "Research Directions in Sparse Matrix Computation," AERE Harwell report, 1982.
10. P. M. EAGLES, *J. Fluid Mech.* **62** (1974), 1–9.
11. H. FASEL AND O. BOOZ, *J. Fluid Mech.* **138** (1984), 21–52.
12. D. R. FEARN AND M. R. E. PROCTOR, *J. Fluid Mech.* **128** (1983), 21–36.
13. L. FOX AND I. B. PARKER, "Chebyshev Polynomials in Numerical Analysis," Oxford Univ. Press, London/New York, 1968.
14. M. Y. HUSSAINI, M. D. SALAS, AND T. A. ZANG, ICASE Preprint No. 17217, 1984; submitted for publication.
15. A. JENNINGS, *Comput. J.* **9** (1966), 281–285.
16. C. A. JONES, *J. Fluid Mech.* **157** (1985), 135–162.
17. C. A. JONES, *J. Fluid Mech.* **102** (1981), 249–261.
18. C. A. JONES, *J. Fluid Mech.* **120** (1982), 433–450.
19. G. P. KING, Y. LI, W. LEE, H. L. SWINNEY, AND P. S. MARCUS, *J. Fluid Mech.* **141** (1984), 365–390.
20. A. LORENZEN, G. PFISTER, AND T. MULLIN, *Phys. Fluids* **26** (1982), 1.
21. P. MARCUS, Simulation of Taylor–Couette flow. I. Numerical methods and comparison with experiment, MIT preprint, 1983.
22. K. A. MEYER, *Phys. Fluids Suppl. II* **12** (1969), 165–170.
23. R. MEYER-SPASCHE AND H. B. KELLER, *J. Comput. Phys.* **35** (1980), 100–109.
24. R. P. MOSER, P. MOIN, AND A. LEONARD, A spectral numerical method for the Navier–Stokes equations with applications to Taylor–Couette flow, Stanford University preprint, 1983.
25. M. NAGATA AND F. H. BUSSE, *J. Fluid Mech.* **135** (1983), 1–26.
26. C. NAKAYA, *J. Phys. Soc. Japan* **38** (1975), 576–585.
27. S. A.ORSZAG, *J. Fluid Mech.* **50** (1971), 689–703.
28. K. PARK, Private communication, 1981.

29. G. O. ROBERTS, *Geophys. Astrophys. Fluid Dynamics* **8** (1977), 187.
30. G. O. ROBERTS, *Geophys. Astrophys. Fluid Dynamics* **12** (1979), 235.
31. E. H. ROGERS AND D. W. BEARD, *J. Comput. Phys.* **4** (1969), 1–18.
32. G. I. TAYLOR, *Philos. Trans. Soc. London, Ser. A* **223** (1923), 289–343.
33. J. H. WILKINSON, "The Algebraic Eigenvalue Problem," Oxford Univ. Press, London/New York, 1965.
34. T. A. ZANG, Y. S. WONG, AND M. Y. HUSSAINI, *J. Comput. Phys.* **54** (1984), 489–507.